FLOODPLAIN SEDIMENTOLOGY AND SEDIMENT ACCUMULATION ASSESSMENT – SAVANNAH RIVER SITE

FINAL REPORT

January 3, 2016

Dr. Kevin M. Yeager
Department of Earth and Environmental Sciences
University of Kentucky
Lexington, KY 40506

1. INTRODUCTION

The primary goal of the larger research program, of which this work is one component, is to restore the hydrodynamics and energy gradients of targeted Savannah River Site (SRS) streams to a condition comparable to local natural streams or rivers of similar order, and to stabilize sediment transport (net degradation/aggregation) with the assumption that the faunal components of these systems will quickly recover on their own (e.g., Pen Branch; Lakly and McArthur, 2000). This work is specifically focused on the identification of near-stream floodplain areas that exhibit sediment deposition or erosion, and the quantification of these processes over a historical time scale (last ~100 years).

2. MATERIALS AND METHODS

2.1 Fieldwork and Sample Processing

During the field season of 2014 (July 21-22), eight sediment coring stations were established and sampled throughout the SRS. A ninth coring station was established during the 2015 field season, but complete results for this station are not yet available. The field campaigns were organized in cooperation with Dr. Chris Barton, were led by myself, and involved graduate students from both Dr. Barton's and my research programs at the University of Kentucky (UK). At each site, sediment cores were collected in duplicate (16 cores total) utilizing vibracoring, a common sediment coring method (e.g., Ward *et al.*, 2008; Pre *et al.*, 2011; Yeager *et al.*, 2012). These stations were distributed throughout the SRS, and their locations were chosen based on (1) preliminary data gathered by Dr. Barton's research group, and (2) the ability to collect relatively undisturbed sediments on floodplains in close proximity (generally within 10-15 m) to perennial streams (Fig. 1).

All sediment cores were then returned to the Sedimentary and Environmental Radiochemistry Research Laboratory (SER_2L; www.ser2l.com), Department of Earth and Environmental Sciences at UK. Both sediment cores from each station were split longitudinally and visually inspected. One core was then selected, with the objective being to select the one core that appeared least disturbed based on observation of the sedimentary section sampled. To balance the desire for high data resolution with a reasonable number of total samples per core, each core was sectioned at a 1 cm interval from the surface to 50 cm depth, and at a 2 cm interval from 50 cm to the end of each core.

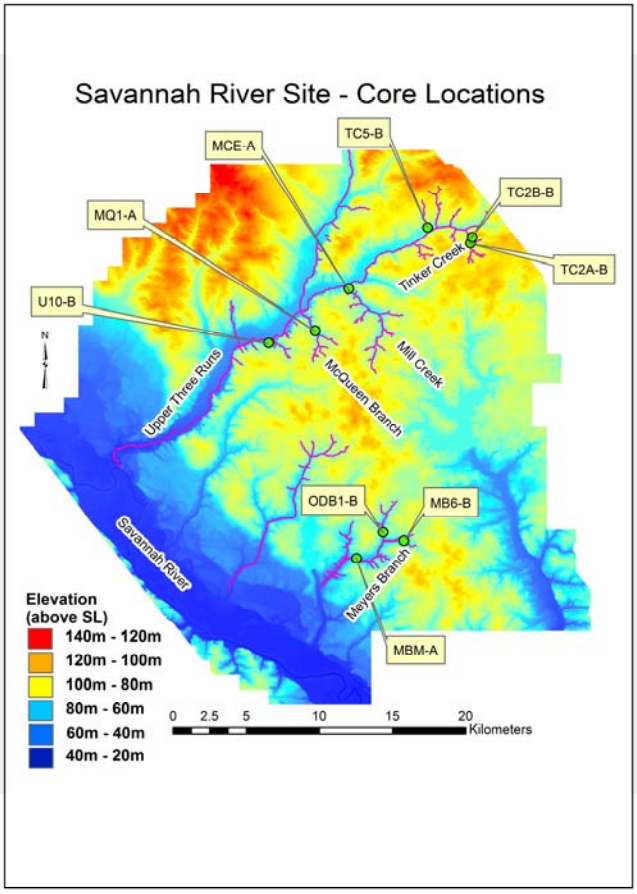

Figure 1: Savannah River Site coring stations (green symbols). LiDAR data courtesy of Dean Fletcher, SRS.

2.2 Physical Variables

Sediments from each core interval were weighed, dried, and re-weighed to determine a range of physical variables, including dry bulk density (B_d), fraction of water (f_w), sediment porosity (ϕ), sediment mass depth and cumulative mass depth. Sediment grain density (ρ_s) was assumed (2.50 g cm^{-3}). The calculations for each of these variables are described in Appendix A. Sediment textures (grain size) were assessed by quantifying the mineral grain size distribution, and sand : silt : clay fractions as defined by the Wentworth Scale (Wentworth, 1922). Grain size samples were dried at ~75 °C for 24 h, gently disaggregated, wet-sieved through 2 and 0.5 mm sieves and treated with dilute H_2O_2 to destroy organic binding agents. Samples are then analyzed using a Malvern Mastersizer, a laser-optical particle size characterization instrument capable of accurately resolving particles over a size range of 0.02 to 2000 µm. Concentrations of particulate organic carbon (POC) were determined via elemental analysis according to methods given in Santschi *et al.* (2001).

2.3 Radiochemistry

High-resolution gamma spectrometry was employed to resolve ^{7}Be ($t_{1/2}$ = 53 d, E_γ = 477 keV), ^{137}Cs ($t_{1/2}$ = 30 y, E_γ = 661 keV) and ^{226}Ra ($t_{1/2}$ = 1,601 y, E_γ = 352 keV) using Canberra HPGe well detectors and multi-channel analyzer, model DSA-1000. Samples were contained in plastic test tubes (inner diameter 1.3 cm, height 9.4 cm), and standards (^{137}Cs and ^{226}Ra: NIST, SRM #4357; ^{7}Be: Isotope Products Laboratories CN #6007) were prepared and run on each detector in geometries identical to those for sediment samples to determine representative efficiencies. Efficiency errors based on standards were less than ± 5%, and samples were counted, on average, for three to four days to reach a standard deviation for all isotopes of ~5%. All activities were decay-corrected to the date of collection. Alpha spectrometry was employed to resolve ^{210}Pb ($t_{1/2}$ = 22.3 y) via ^{210}Po using a Canberra integrated alpha spectrometer, model 7200. Lead-210 samples were spiked with a certified ^{209}Po tracer (Isotope Products Laboratory, #6209-100N) and completely digested (HF, HCl, HNO_3) over heat. Ascorbic acid was then added to bind free Fe (III), and a silver disk was added to the solution over heat to provide a substrate for the spontaneous deposition of polonium isotopes (Santschi *et al.*, 1999; Yeager *et al.*, 2004, 2007, 2012). Unsupported, or "excess" ^{210}Pb ($^{210}Pb_{xs}$) is determined by $^{210}Pb_{xs}$ = Total ^{210}Pb – ^{226}Ra-supported ^{210}Pb, where the supported ^{210}Pb fraction is estimated as the mean total ^{210}Pb at the bottom of each sediment core profile.

2.4 Sediment Accumulation Modeling

The constant fallout radionuclide ^{7}Be has been used successfully to assess depths of short-term (~1 year) sediment mixing in a range of terrestrial and aquatic settings (e.g., Clifton *et al.*, 1995; Wheatcroft and Drake, 2003; Yeager *et al.*, 2004, 2012), and was utilized here for all eight stations.

Sediment accumulation rates have been determined in a range of terrestrial and aquatic settings using the bomb-fallout radionuclide ^{137}Cs (e.g., DeLaune *et al.*, 1978; Edgington *et al.*, 1991; Fuller *et al.*, 1999; Yeager *et al.*, 2006), and are determined here by:

$$S = (D_{pk}/t) \quad (1)$$

where S = sediment accumulation rate (cm y^{-1}), D_{pk} = depth at which the maximum ^{137}Cs activity concentration occurs (1963), or alternatively, the first time that ^{137}Cs can be determined (1952), and t = time. This model assumes limited vertical mobility of ^{137}Cs in sediments (Huntley *et al.*, 1995; Winkels *et al.*, 1998; Valero-Garces *et al.*, 1999).

As with ^{137}Cs, ^{210}Pb has been widely employed to determine sediment geochronology and rates of sediment accumulation in many terrestrial and aquatic settings (e.g., Carpenter *et al.*, 1985; Schuler *et al.*, 1991; Santschi *et al.*, 1999; Yeager *et al.*, 2004). Since these stream floodplains are only periodically inundated, sediment accumulation rates were determined using the constant flux model (Appleby and Oldfield, 1978, 1992; Appleby, 2008). This model is appropriate for settings such as these, where ^{210}Pb fallout may be constant, but sedimentation is not. The $^{210}Pb_{xs}$ distribution as a function of mass depth is:

$$^{210}Pb_{xs} = F_{210}e^{-\lambda t}/S_a \quad (2)$$

where F_{210} = flux of ^{210}Pb, λ = ^{210}Pb decay constant (0.031 y^{-1}), t = time, and S_a = sediment mass accumulation rate (MAR) (g cm^{-2} y^{-1}). The sediment MAR as a function of mass depth is:

$$S_a = \Delta m/\Delta t \quad (3)$$

where m = mass depth (g cm^{-2}).

3. RESULTS

Sediment mixing depths and accumulation rates are shown in Table 1. Profiles of ^{7}Be indicate that physical and/or biological sediment mixing is not evident at five of the eight stations. The three stations that do exhibit detectable activity concentrations of ^{7}Be (U10-B, TC2A-B, and TC2B-B) indicate that near-term sediment mixing is restricted to the upper 1-2 cm of the sediment profiles. Results for each station are highlighted in turn below.

Table 1: Organic carbon inventories (to 30 cm), near term sediment mixing (^{7}Be; 1 year), and sediment accumulation rate results based on ^{137}Cs and $^{210}Pb_{xs}$. For [All] and [Selected], please see the text for each station; all uncertainties reported at 1-sigma.

Station	POC inventory (g cm^{-2})	POC flux (g cm^{-2} y^{-1})	^{7}Be mixed depth (cm)	^{137}Cs sediment accumulation rates (*g cm^{-2} y^{-1}*; cm y^{-1})	$^{210}Pb_{xs}$ mean sediment accumulation rates (*g cm^{-2} y^{-1}*; cm y^{-1})
U10-B	0.53	0.03 ± 0.01	1	*0.47 ± 0.09*; 0.30 ± 0.02	*1.54 ± 1.65*; 1.01 ± 1.08 [All]; *0.45 ± 0.24*; 0.29 ± 0.16 [Selected]
MBM-A	0.23	0.01 ± 0.01	0	*0.37 ± 0.07*; 0.25 ± 0.02	*0.17 ± 0.05*; 0.14 ± 0.04
ODB-1B	0.75	0.07 ± 0.03	0	*0.16 ± 0.03*; 0.17 ± 0.02	*0.32 ± 0.18*; 0.21 ± 0.12
TC5-B	1.86	0.04 ± 0.03	0	*0.13 ± 0.02*; 0.25 ± 0.02	*0.19 ± 0.19*; 0.46 ± 0.46
MQ1-A	0.69	0.02 ± 0.01	0	*0.37 ± 0.06*; 0.30 ± 0.02	*0.46 ± 0.25*; 0.31 ± 0.17
TC2A-B	1.08	0.07 ± 0.03	1	*0.24 ± 0.05*; 0.35 ± 0.02	*0.22 ± 0.11*; 0.33 ± 0.16
MCE-A	0.86	0.05 ± 0.02	0	*0.24 ± 0.05*; 0.23 ± 0.01	*0.22 ± 0.12*; 0.15 ± 0.08
TC2B-B	1.44	0.03 ± 0.01	2	*0.08 ± 0.02*; 0.19 ± 0.01	*0.14 ± 0.05*; 0.18 ± 0.06

3.1 Station U10-B

Limited short-term mixing is evident at this station based on the penetration of ^{7}Be (1 cm). The sediment here is dominantly sand-size, with increasing silt- and clay-size sediment between 20-30 cm, and from 10 cm to the surface (Fig. 2), two intervals that likely reflect discrete floodplain depositional periods. The POC profile for this station exhibits a typical exponential decline with depth (Fig. 3), yielding a POC inventory of 0.53 g cm^{-2}. The profile of ^{137}Cs (Fig. 4) does not exhibit a clear peak, so mean sediment accumulation was determined using the first appearance of above-background ^{137}Cs (1952; Table 1). Examining the change in sediment accumulation rates over time as determined using $^{210}Pb_{xs}$ (Fig. 5) shows that while rates appear to have been steadily increasing over the entire period of record, a major and sustained depositional event occurred between ~30-10 years ago, with sediment accumulation increasing by more than a factor of six. The mean sediment accumulation rates derived using the entire $^{210}Pb_{xs}$ data set are much higher than those derived using ^{137}Cs, but with large uncertainties produced by the pulsed sedimentation event. Removing this event, the remaining data show long-term rates of sediment accumulation in strong agreement with those determined using ^{137}Cs (Fig. 6; Table 1). Using the surface POC concentration and long-term mean sediment accumulation rate (excluding the pulsed sedimentation event) allows for a POC flux of 0.03 ± 0.01 g cm^{-2} y^{-1} to be determined.

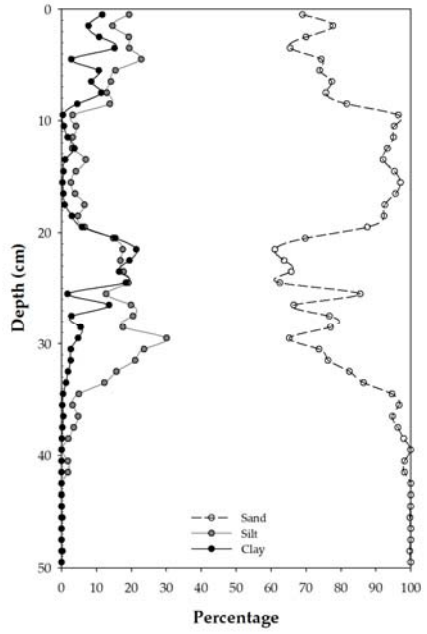

Figure 2: U10-B-14V grain size distribution.

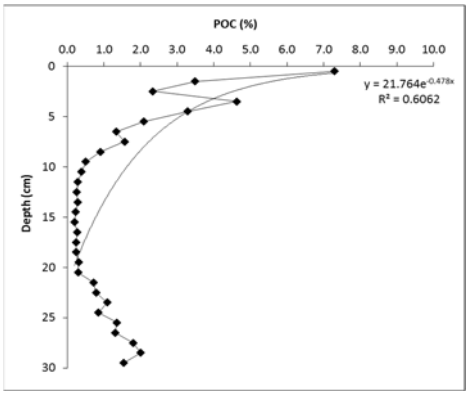

Figure 3: U10-B-14V POC profile.

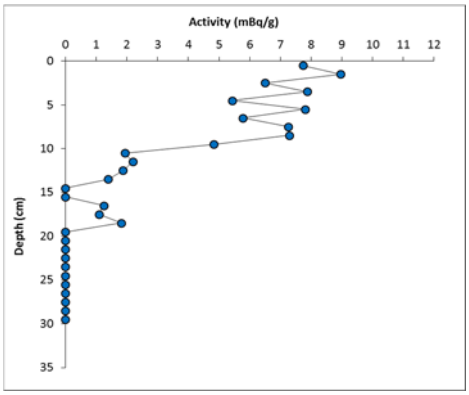

Figure 4: U10-B-14V ^{137}Cs profile.

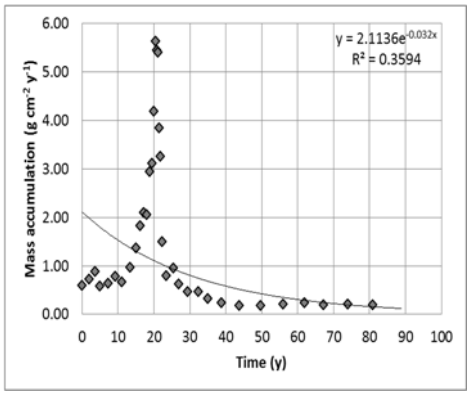

Figure 5: U10-B-14V sediment accumulation rates over time based on $^{210}Pb_{xs}$ [All].

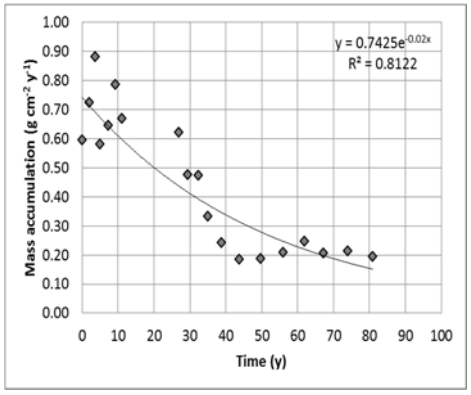

Figure 6: U10-B-14V sediment accumulation rates over time based on $^{210}Pb_{xs}$ [Selected].

3.2 Station MBM-A

No short-term mixing is evident at this station based on the penetration of ^{7}Be. The sediment here has a chaotic grain size distribution from ~50-30 cm, then becomes dominantly sand-size, with a small increase in silt and clay sized sediment from 10 cm to the surface (Fig. 7). The POC profile for this station exhibits a typical exponential decline with depth (Fig. 8), yielding a POC inventory of 0.23 g cm^{-2}.

The profile of ^{137}Cs (Fig. 9) does not exhibit a clear peak, so mean sediment accumulation was determined using the first appearance of above-background ^{137}Cs (1952; Table 1). Examining the change in sediment accumulation rates over time as determined using $^{210}Pb_{xs}$ (Fig. 10) shows that rates appear to have been steadily increasing over the entire period of record. The mean sediment accumulation rates derived using $^{210}Pb_{xs}$ are somewhat lower than those

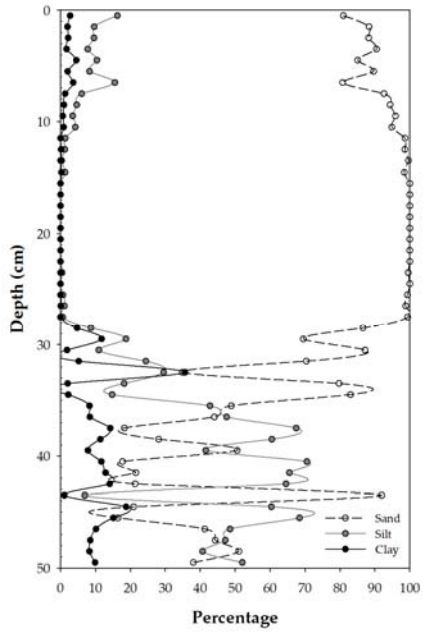

Figure 7: MBM-A-14V grain size distribution.

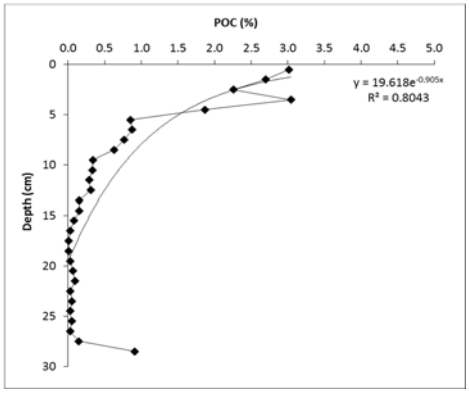

Figure 8: MBM-A-14V POC profile.

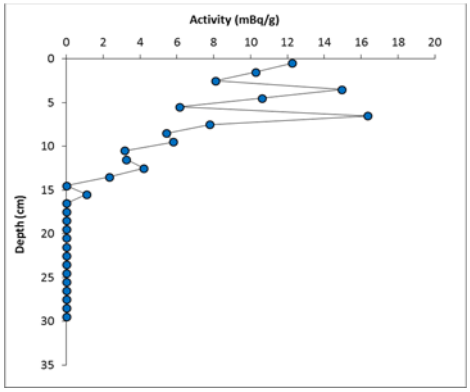

Figure 9: MBM-A-14V ^{137}Cs profile.

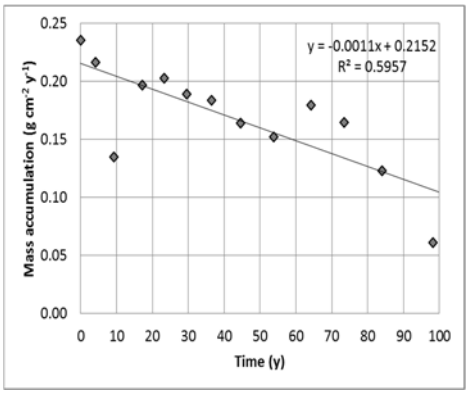

Figure 10: MBM-A-14V sediment accumulation rates over time based on $^{210}Pb_{xs}$.

derived using ^{137}Cs, reflecting progressively increasing rates of sediment accumulation, and the differences between the time frames resolved using ^{137}Cs (last ~50-60 years) and $^{210}Pb_{xs}$ (last ~100 years). Using the surface POC concentration and long-term mean sediment accumulation rate allows for a POC flux of 0.01 $\pm$ 0.01 g cm^{-2} y^{-1} to be determined.

3.3 Station ODB-1B

No short-term mixing is evident at this station based on the penetration of ^{7}Be. The sediment here is dominantly sand-size, with an increase in silt- and clay-sized sediment from 15-5 cm, with the sand-sized fraction again increasing from 5 cm to the surface (Fig. 11). The POC profile for this station exhibits a typical exponential decline with depth (Fig. 12), yielding a POC inventory of 0.75 g cm^{-2}.

The profile of ^{137}Cs (Fig. 13) exhibits a clear peak, which was utilized to derive mean sediment accumulation rates (1963; Table 1). Examining sediment accumulation rates over time as determined using $^{210}Pb_{xs}$ (Fig. 14) shows that rates appear to have been steady over much of the period of record, with the exception of two pulsed sedimentation events occurring between ~90-60 years ago, and another between ~20-10 years ago, with sediment accumulation increasing by more than a factor of four in the first event, and by a factor of three in the second event. The mean sediment accumulation rates derived using the entire $^{210}Pb_{xs}$ data set are higher than those derived using ^{137}Cs, but with large uncertainties produced by the pulsed sedimentation events.

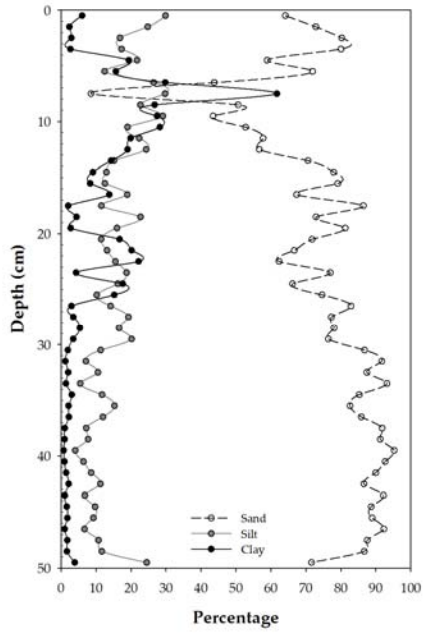

Figure 11: ODB-1B-14V grain size distribution.

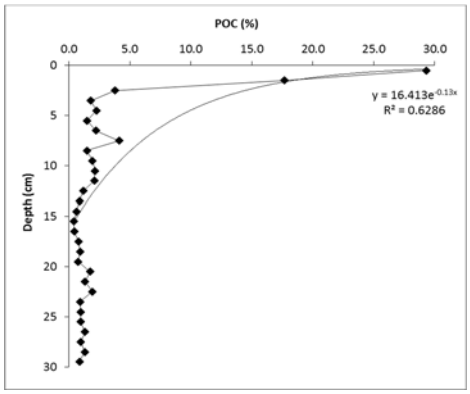

Figure 12: ODB-1B-14V POC profile.

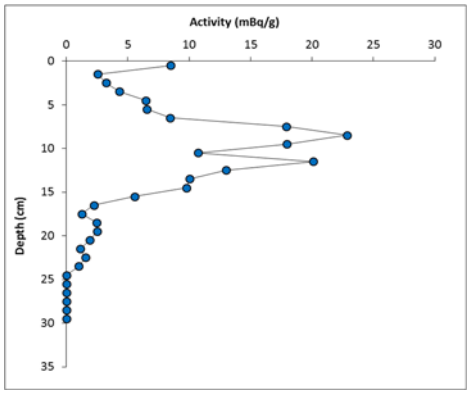

Figure 13: ODB-1B-14V ^{137}Cs profile.

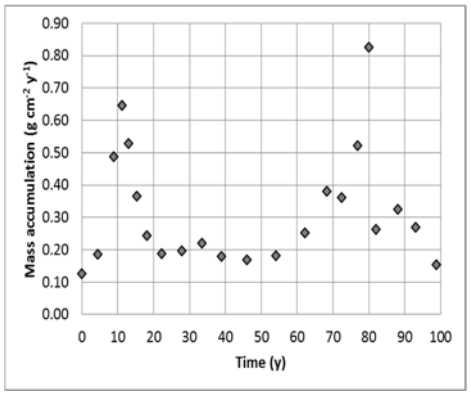

Figure 14: ODB-1B-14V sediment accumulation rates over time based on $^{210}Pb_{xs}$.

Using the surface POC concentration and long-term mean sediment accumulation rate allows for a POC flux of 0.07 $\pm$ 0.03 g cm^{-2} y^{-1} to be determined.

3.4 Station TC5-B

No short-term mixing is evident at this station based on the penetration of ^{7}Be. The sediment here is dominantly sand-size from 50 to 20 cm depth, then becomes dominantly silt-sized from 20 to 5 cm depth, and finally is mixed sand- and silt-sized from 5 cm to the surface (Fig. 15). The POC profile for this station exhibits a typical exponential decline with depth (Fig. 16), yielding a POC inventory of 1.86 g cm^{-2}.

The profile of ^{137}Cs (Fig. 17) exhibits a peak near to the surface (2.5 cm), but the truncation of the full profile near the surface suggests erosion of surface sediment. As such, mean sediment accumulation was determined using the first appearance of above-background ^{137}Cs (1952; Table 1). Examining sediment accumulation rates over time as determined using $^{210}Pb_{xs}$ (Fig. 18) shows that rates appear to have been steadily increasing over the period of record, with the exception of a pulsed sedimentation event occurring between ~35-20 years ago, with sediment accumulation increasing by a factor of eight during this event. The timing of this event should be interpreted with some caution, given the evidence of erosion at this station. The mean sediment accumulation rates derived using the entire $^{210}Pb_{xs}$ data set are somewhat higher than those derived using ^{137}Cs, but with large uncertainties produced

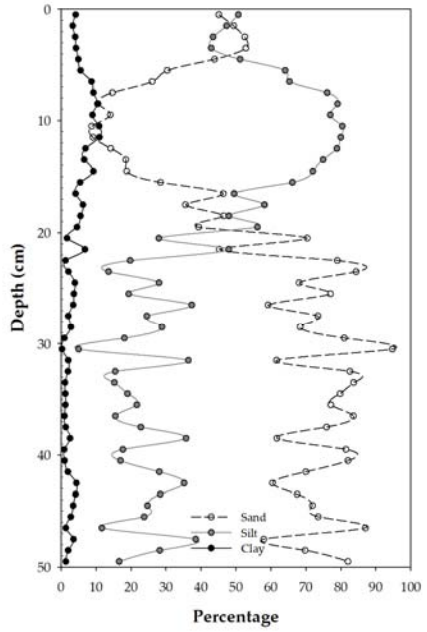

Figure 15: TC5-B-14V grain size distribution.

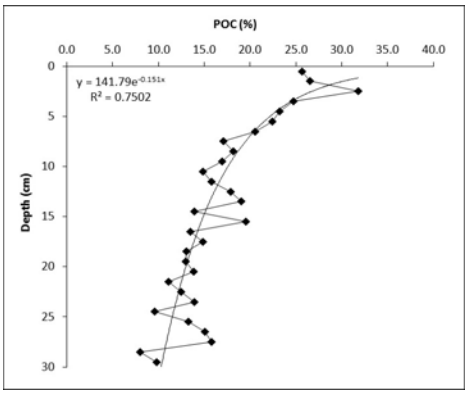

Figure 16: TC5-B-14V POC profile.

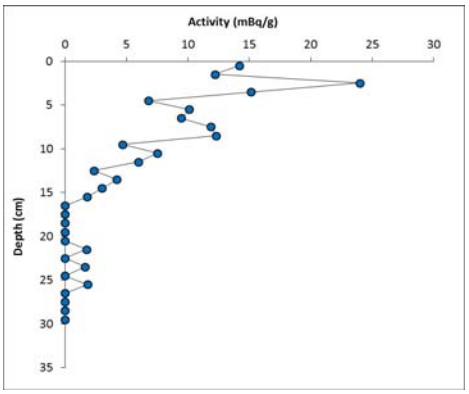

Figure 17: TC5-B-14V ^{137}Cs profile.

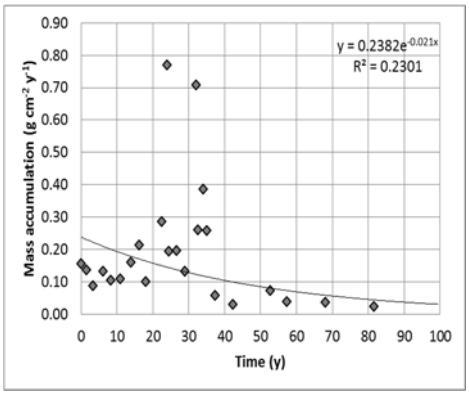

Figure 18: TC5-B-14V sediment accumulation rates over time based on $^{210}Pb_{xs}$.

by the pulsed sedimentation event. Using the surface POC concentration and long-term mean sediment accumulation rate allows for a POC flux of 0.04 $\pm$ 0.03 g cm^{-2} y^{-1} to determined.

3.5 Station MQ1-A

No short-term mixing is evident at this station based on the penetration of ^{7}Be. The sediment here is dominantly sand-size, particularly from 30 to 50 cm depth, from 30 cm to 20 cm the sediment becomes progressively more silt-sized, and from 20 cm to the surface, the size distributions between clay, silt and sand-sized sediment remains static (Fig. 19). The POC profile for this station exhibits a typical, approximately exponential decline with depth (Fig. 20), yielding a POC inventory of 0.69 g cm^{-2}.

The profile of ^{137}Cs (Fig. 21) exhibits a clear peak, which was utilized to derive mean sediment accumulation rates (1963; Table 1). Examining sediment accumulation rates over time as determined using $^{210}Pb_{xs}$ (Fig. 22) shows that rates appear to have been steady until approximately 50 years ago, when they began to rapidly increase. The mean sediment accumulation rates derived using the entire $^{210}Pb_{xs}$ data set agree well with those derived using ^{137}Cs (within the uncertainties). Using the surface POC concentration and long-term mean sediment accumulation rate allows for a POC flux of 0.02 $\pm$ 0.01 g cm^{-2} y^{-1} to be determined.

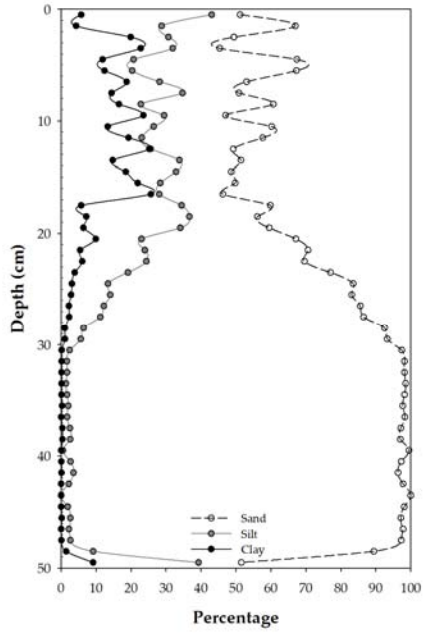

Figure 19: MQ1-A-14V grain size distribution.

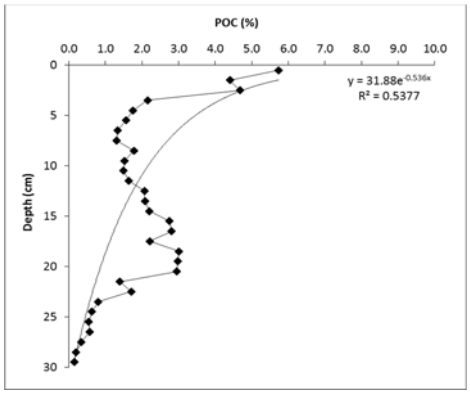

Figure 20: MQ1-A-14V POC profile.

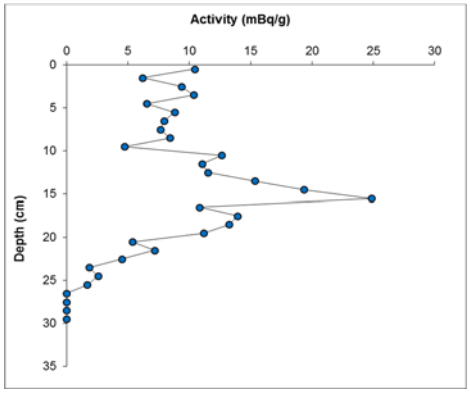

Figure 21: MQ1-A-14V ^{137}Cs profile.

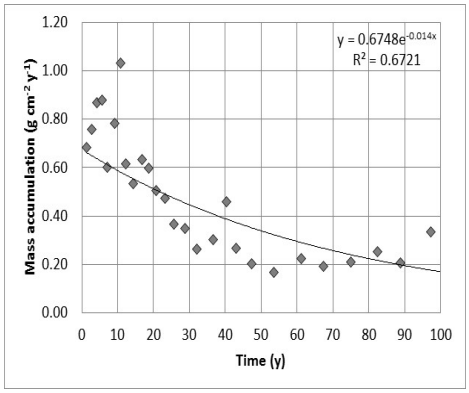

Figure 22: MQ1-A-14V sediment accumulation rates over time based on $^{210}Pb_{xs}$.

3.6 Station TC2A-B

Limited short-term mixing is evident at this station based on the penetration of ^{7}Be (1 cm). The sediment here is dominantly sand-size, but becomes progressively enriched in silt-sized sediment from 20 cm to the surface (Fig. 23). The POC profile for this station exhibits a typical exponential decline with depth (Fig. 24), yielding a POC inventory of 1.08 g cm^{-2}.

The profile of ^{137}Cs (Fig. 25) does not exhibit a clear peak, so mean sediment accumulation was determined using the first appearance of above-background ^{137}Cs (1952; Table 1). The irregular appearance of the ^{137}Cs profile, including the absence of a top limb of the profile suggest that some erosion has taken place at this site. Examining sediment accumulation rates over time as determined using $^{210}Pb_{xs}$ (Fig. 26) shows that rates appear to have been steadily increasing from approximately 90 years ago to 30 years ago, after which they have dropped off considerably. This trend may reflect a major reduction in sedimentation, or may reflect the removal of near-surface sediments by erosion. The mean sediment accumulation rates derived using the entire $^{210}Pb_{xs}$ data set agree well with those derived using ^{137}Cs. Using the surface POC concentration and long-term mean sediment accumulation rate allows for a POC flux of 0.07 $\pm$ 0.03 g cm^{-2} y^{-1} to be determined.

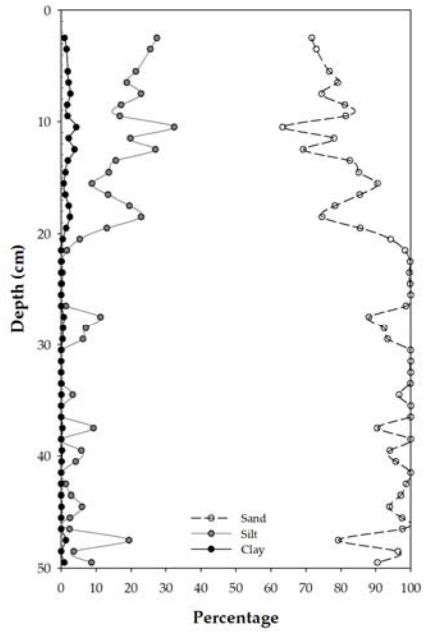

Figure 23: TC2A-B-14V grain size distribution.

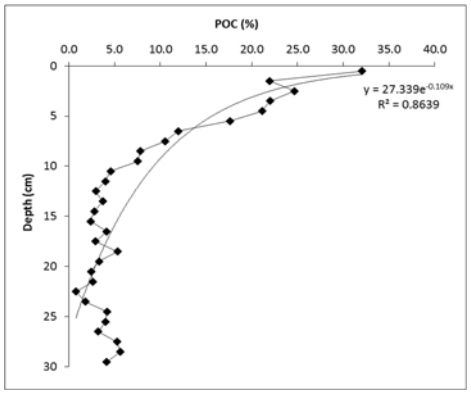

Figure 24: TC2A-B-14V POC profile.

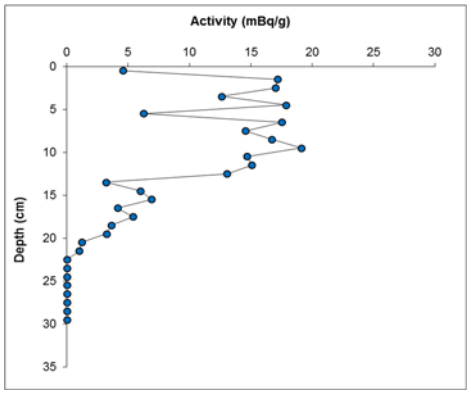

Figure 25: TC2A-B-14V ^{137}Cs profile.

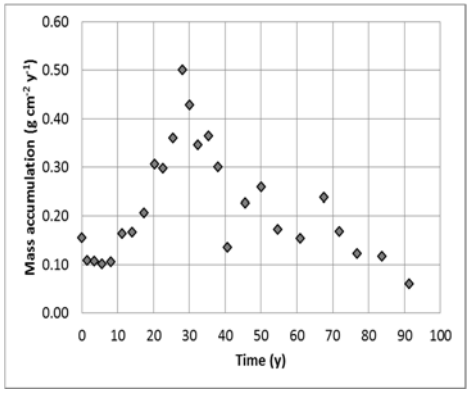

Figure 26: TC2A-B-14V sediment accumulation rates over time based on $^{210}Pb_{xs}$.

3.7 Station MCE-A

No short-term mixing is evident at this station based on the penetration of ^{7}Be. The sediment here is dominantly sand-size over the entire section, with the exception of a punctuated spike in clay- and silt-sized sediment at approximately 27-30 cm depth, which is likely associated with a floodplain depositional event (Fig. 27). The POC profile for this station exhibits a typical exponential decline with depth (Fig. 28), yielding a POC inventory of 0.86 g cm^{-2}.

The profile of ^{137}Cs (Fig. 29) does exhibit a peak within 5 cm of the surface, but the irregular form of the profile, and the absence of the upper limb of the profile suggests erosion at this site. As such, mean sediment accumulation was determined using the first appearance of above-background ^{137}Cs (1952; Table 1). Examining sediment accumulation rates over time as determined using $^{210}Pb_{xs}$ (Fig. 30) shows that rates appear to have been steadily declining over most of the period of record. The mean sediment accumulation rates derived using the entire $^{210}Pb_{xs}$ data set agree well with those derived using ^{137}Cs. Using the surface POC concentration and long-term mean sediment accumulation rate allows for a POC flux of 0.05 $\pm$ 0.02 g cm^{-2} y^{-1} to be determined.

3.8 Station TC2B-B

Limited short-term mixing is evident at this station based on the penetration of ^{7}Be (2 cm), though this is the deepest mixing evident at any of these sites. The sediment here is

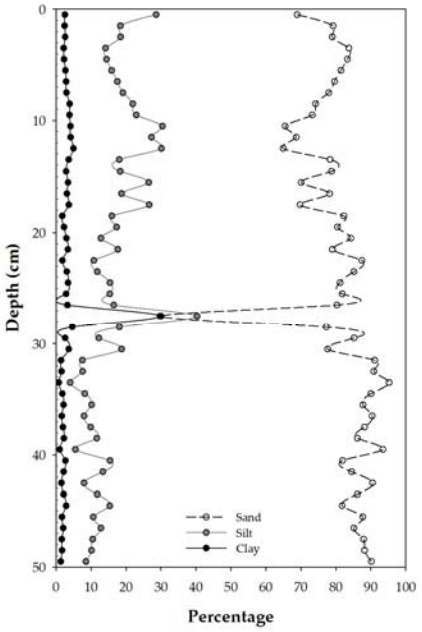

Figure 27: MCE-A-14V grain size distribution.

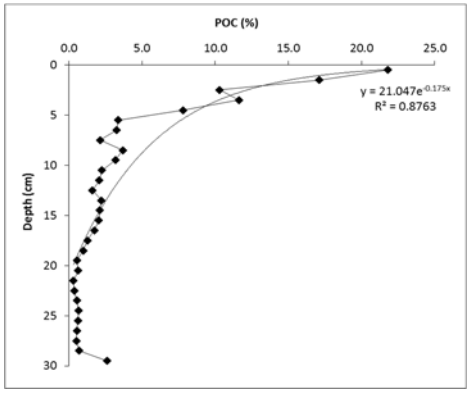

Figure 28: MCE-A-14V POC profile.

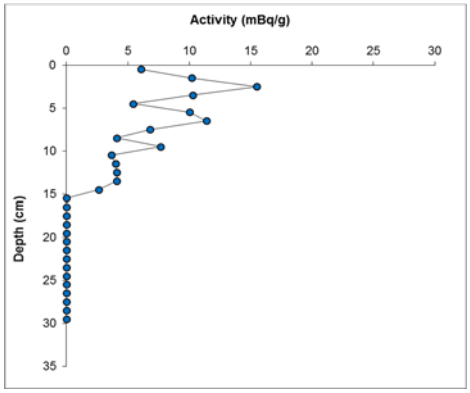

Figure 29: MCE-A-14V ^{137}Cs profile.

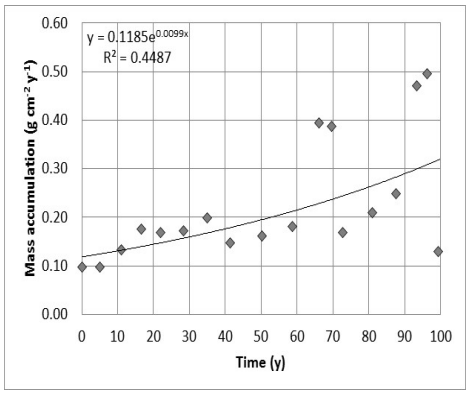

Figure 30: MCE-A-14V sediment accumulation rates over time based on $^{210}Pb_{xs}$.

dominantly sand-size over most of the section, but becomes progressively enriched with silt-sized sediment from 20 cm depth to the surface (Fig. 31). The POC profile for this station exhibits a typical exponential decline with depth (Fig. 32), yielding a POC inventory of 1.44 g cm^{-2}.

The profile of ^{137}Cs (Fig. 33) does exhibit a peak within 5 cm of the surface, but the irregular form of the profile, and the absence of the upper limb of the profile suggests erosion at this site. As such, mean sediment accumulation was determined using the first appearance of above-background ^{137}Cs (1952; Table 1). Examining sediment accumulation rates over time as determined using $^{210}Pb_{xs}$ (Fig. 34) shows that rates appear to have been steadily increasing from approximately 90 to 30 years ago, and then slowed appreciably and have remained static. The mean sediment accumulation rates derived using the entire $^{210}Pb_{xs}$ data set agree well with those derived using ^{137}Cs. Using the surface POC concentration and long-term mean sediment accumulation rate allows for a POC flux of 0.03 $\pm$ 0.01 g cm^{-2} y^{-1} to be determined.

4. CONCLUSIONS

Aerial photos from 1938 and 1951 show that much of the upland areas and terraces along Tinker Creek and its tributaries were used for agriculture, and since 1951 have been converted and managed as forestland (Fletcher *et al*., 2012). The general increase in sediment mass accumulation rates within the Tinker Creek watershed (TC2A-B, TC2B-B,

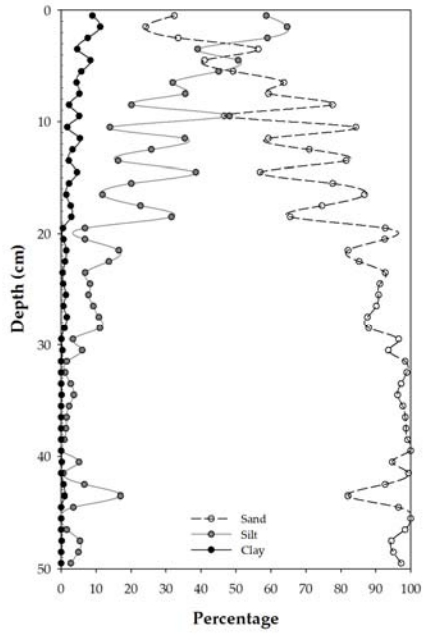

Figure 31: TC2B-B-14V grain size distribution.

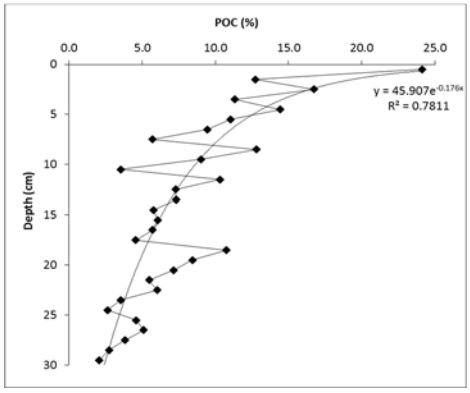

Figure 32: TC2B-B-14V POC profile.

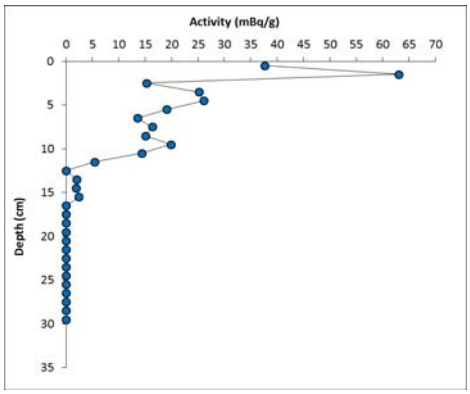

Figure 33: TC2B-B-14V ^{137}Cs profile.

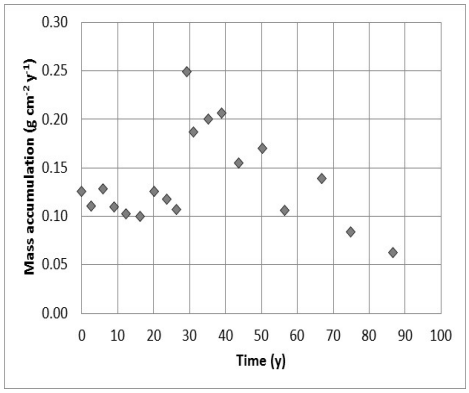

Figure 34: TC2B-B-14V sediment accumulation rates over time based on $^{210}Pb_{xs}$.

and TC5-B) may be a response to revegetation efforts. Plots of mean sediment accumulation over time as determined using $^{210}Pb_{xs}$ for all three stations show a disturbance in this trend approximately 35-40 years ago. There was a dam present just below TC2A-B and TC2B-B in the 1951 aerial imagery, which inundated the area with water in what was then-known as "Kennedy Pond". The Stream Condition Survey Final Report does not mention in what year after 1951 this dam was breached, but if it was approximately 40 years ago, that could explain the considerable drop in sedimentation rates at both TC2A-B and TC2B-B, as well as the large increase in sediment accumulation at TC5-B, which is downstream of the former "Kennedy Pond" area.

MCE-A is the only coring station to show a systematic decrease in sediment accumulation rates. This station is located at the confluence of Mill Creek and Upper Three Runs, and is therefore reflective of the entire 23.4 km^2 drainage area. This area is characterized by 39 flow impediments, 29 of which were of pre-SRS origin, while 10 resulted from SRS activities. These impediments include active and abandoned road crossings, six abandoned dams (only one of which was still active in the 1951 aerial photos), and both active and abandoned beaver dams. It was noted in the Stream Condition Survey Final Report that beavers have often plugged the breaches in the abandoned dams and levees along this stream, resulting in a greater

accumulation of fine sediment upstream of this coring station. This may explain the decrease in sediment accumulation at this coring station, as well as the irregularity of the decrease as these structures are periodically removed by the SRS.

The main stem of the Meyers Branch stream (ODB-1B and MBM-A) has had significant impacts derived from both pre-SRS and post-SRS activities (41 and 7 impacts, respectively). Meyers Branch was impacted by roads, railroads, and the Dunbarton community, which was established in the early 1800s. These impacts include the construction of a railroad in 1899 that hydrologically isolated the northern and southern halves of the drainage basin, until it was moved in the 1950s. Between 1951 and 1955, several ditches were constructed to carry stormwater runoff from the P Area and the Railroad Yard (Fletcher *et al*., 2012). These efforts may explain the change in the slope of sediment accumulation as determined by $^{210}Pb_{xs}$ at MBM-A (Fig. 10) before and after ~65 years ago.

Nearly the entire valley of the U10-B watershed was forested pre-SRS, although the upland areas had been used for agriculture. Since the floodplains were already vegetated, the revegetation efforts of the SRS in this basin had minimal impact on the sediment accumulation rates. The basin is characterized by steep slopes and its proximity to the H Area borrow pit (Fletcher *et al.*, 2012). The punctuated increase in sediment accumulation ~20 years ago was most likely caused by slope failure, and the subsequent landslide of sediment being deposited in the stream either by the borrow pit or the sides of the valley.

5. RESEARCH DISSEMINATION

This research is a primary component of one M.S. thesis in Geological Sciences, now in progress, with completion anticipated in the summer, 2016. The completed work will also be presented at the national Geological Society of America meeting in September, 2016. Once this work is integrated with the other components of the overall research project, we anticipate producing at least one and perhaps several peer-reviewed publications in international journals, which may include *Water Resources Research*, *Earth Surface Processes and Landforms* or *Catena*.

6. LITERATURE CITED

Appleby, P.G., 2008. Three decades of dating recent sediments by fallout radionuclides: A review. *The Holocene* 18(1): 83-93.

Appleby, P.G., F. Oldfield, 1978. The calculation of lead-210 dates assuming a constant rate of supply of unsupported ^{210}Pb to the sediment. *Catena* 5: 1–8.

Appleby, P.G., F. Oldfield, 1992. Application of lead-210 to sedimentation studies. In: Ivanovich, M., R.S. Harman, (Eds.), *Uranium-Series Disequilibrium: Application to Earth, Marine, and Environmental Sciences*. Clarendon Press, Oxford, p. 731–778.

Carpenter, R., M.L. Peterson, J.T. Bennett, 1985. ^{210}Pb-Derived sediment accumulation and mixing rates for the greater Puget Sound region. *Marine Geology* 64(3-4): 291-312.

Clifton, R.J., P.G. Watson, J.T. Davey, P.E. Frickers, 1995. A study of processes affecting the uptake of contaminants by intertidal sediments, using the radioactive tracers: ^{7}Be, ^{137}Cs and unsupported ^{210}Pb. *Estuarine, Coastal and Shelf Science* 41(4): 459-474.

DeLaune, R.D., W.H. Patrick Jr., R.J. Buresh, 1978. Sedimentation rates determined by ^{137}Cs dating in a rapidly accreting salt marsh. *Nature* 275: 532-533.

Edgington, D.N., J. val Klump, J.A. Robbins, Y.S. Kusner, V.D. Pampura, I.V. Sandimirov, 1991. Sedimentation rates, residence times and radionuclide inventories in Lake Baikal from ^{137}Cs and ^{210}Pb in sediment cores. *Nature* 350: 601-604.

Fletcher, D.E., G. Stillings, C. Barton, 2012. Stream system field condition assessments – level I surveys. Savannah River Ecology Laboratory.

Fuller, C.C., A van Geen, M. Baskaran, R. Anima, 1999. Sediment chronology in San Francisco Bay, California, defined by ^{210}Pb, ^{234}Th, ^{137}Cs, and ^{239,240}Pu. *Marine Chemistry* 64(1-2): 7-27.

Huntley, S.L., R.J. Wenning, S.H. Su, N.L. Bonnevie, D.J. Paustenbach, 1995. Geochronology and sedimentology of the Lower Passaic River, New Jersey. *Estuaries* 18(2): 351–361.

Lakly, M.B., J.V. McArthur, 2000. Macroinvertebrate recovery of a post-thermal stream: Habitat structure and biotic function. *Ecological Engineering* 15 (Suppl 1): 87-100.

Pre, C.G., S.J. Culver, D.J. Mallinson, K.M. Farrell, D.R. Corbett, B.P. Horton, C. Hillier, S.R. Riggs, S.W. Snyder, M.A. Buzas, 2011. Rapid Holocene coastal change revealed by high-resolution micropaleontological analysis, Pamlico Sound, North Carolina, USA. *Quaternary Research* 76(3): 319-334.

Santschi, P.H., L. Guo, S. Asbill, M. Allison, B. Kepple, L.-S. Wen, 2001. Accumulation rates and sources of sediments and organic carbon on the Palos Verdes shelf based on multiple radioisotopic tracers (^{137}Cs, ^{239,240}Pu, ^{210}Pb, ^{234}Th, ^{238}U and ^{14}C). *Marine Chemistry* 73(2): 125-152.

Santschi, P.H., M. Allison, S. Asbill, A.B. Perlet, S. Cappellino, C. Dobbs, L. McShea, 1999. Sediment transport and Hg recovery in Lavaca Bay, as evaluated from radionuclide and Hg distributions. *Environmental Science and Technology* 33: 378 -391.

Schuler, C., E. Wieland, P.H. Santschi, M. Sturm, A. Lueck, S. Bollhalder, J. Beer, G. Bonani, H.J. Hofmann, M. Suter, W. Wolfli, 1991. A multitracer study of radionuclides in Lake Zurich, Switzerland: 1. Comparison of atmospheric and sedimentary fluxes of ^{7}Be, ^{10}Be, ^{210}Pb, ^{210}Po, and ^{137}Cs. *J. of Geophysical Research – Oceans* 96(C9): 17,051-17,065.

Valero-Garces, B., A. Navas, J. Machin, D. Walling, 1999. Sediment sources and siltation in mountain reservoirs: A case study from the Central Spanish Pyrenees. *Geomorphology* 28: 23–41.

Ward, L.G., B.J. Zaprowski, K.D. Trainer, P.T. Davis, 2008. Stratigraphy, pollen history and geochronology

of tidal marshes in a Gulf of Maine estuarine system: Climatic and relative sea level impacts. *Marine Geology* 256(1-4): 1-17.

Wentworth, C.K., 1922. A scale of grade and class terms for clastic sediments. *J. of Geology* 30: 377-392.

Wheatcroft, R.A., D.E. Drake, 2003. Post-depositional alteration and preservation of sedimentary event layers on continental margins, I. The role of episodic sedimentation. *Marine Geology* 199(1-2): 123-137.

Winkels, H., S. Kroonenberg, M. Lychagin, G. Marin, G. Rusakov, N. Kasimov, 1998. Geochronology of priority pollutants in sedimentation zones of the Volga and Danube delta in comparison with the Rhine delta. *Applied Geochemistry* 13(5): 581–591.

Yeager, K.M., C.A. Brunner, M.A. Kulp, D. Fischer, R.A. Feagin, K.J. Schindler, J. Prouhet, G. Bera, 2012. Significance of active growth faulting on marsh accretion processes in the lower Pearl River, Louisiana. *Geomorphology* 153: 127-143.

Yeager, K.M., P.H. Santschi, G.T. Rowe, 2004. Sediment accumulation and radionuclide inventories (^{239,240}Pu, ^{210}Pb and ^{234}Th) in the northern Gulf of Mexico, as influenced by organic matter and macrofaunal density. *Marine Chemistry* 91: 1-14.

Yeager, K.M., P.H. Santschi, H. Rifai, M. Suarez, R. Brinkmeyer, C.-C. Hung, K.J. Schindler, M. Andres, E.A. Weaver, 2007. Dioxin chronology and fluxes in sediments of the Houston Ship Channel, Texas: Influences of non-steady state sediment transport and total organic carbon. *Environmental Science and Technology* 41(15): 5,291-5,298.

Yeager, K.M., P.H. Santschi, K.J. Schindler, M.J. Andres, E.A. Weaver, 2006. The relative importance of terrestrial versus marine sediment sources to the Nueces-Corpus Christi Estuary, Texas: An isotopic approach. *Estuaries and Coasts* 29(3): 443-454.

APPENDIX A

Physical Variables Determined:

(1) Sediment dry bulk density (B_d) – g/cm^3: Determined using a slight modification of the core method, by B_d = mass of dry solids (g)/total volume (cm^3)

(2) Sediment fraction of water (f_w): Determined by f_w = [(sediment wet mass (g)/sediment dry mass (g))/sediment wet mass (g)]

(3) Sediment fraction of organic matter (f_{om}) - %: Determined by f_{om} = [2 x % POC]

(4) Sediment grain density (ρ_s) – g/cm^3: An initial value of 2.50 g/cm^3 is assumed, reflecting a mix of dominantly silicate minerals, and is modified where possible by considering the fraction of sedimentary organic matter (when available) by: ρ_s = [((1.70 g/cm^3 x f_{om}) + (2.50 x (100 – f_{om}))/100]

(5) Sediment porosity (ϕ) - %: Determined by also considering the fraction of sedimentary organic matter (when available) by: ϕ = [(f_w/(f_w + (1 - f_w)/ρ_s)]

(6) Sediment mass depth – g/cm^2: Determined by [(1 - ϕ) x ρ_s x interval thickness (cm)]

(7) Sediment cumulative mass depth – g/cm^2: Determined as the sum of mass depths over depth

(8) Fractions of sand, silt and clay – %: Size classes of mineral sediment corresponding to the Wentworth scale, sand (2 mm – 62.5 μm), silt (62.5 μm – 4 μm) and clay (< 4 μm) (Wentworth, 1922)